Characterization of bio-crude components derived from pyrolysis of soft wood and its esterified product by ultrahigh resolution mass spectrometry and spectroscopic techniques

Diana Catalina Palacio Lozano[1,2], Claudia X. Ramírez[3], José Aristóbulo Sarmiento Chaparro[4], Mary J. Thomas[1,5], Remy Gavard[5], Hugh E. Jones[1,5], Rafael Cabanzo Hernández[2], Enrique Mejia-Ospino[2], Mark P. Barrow[1]

[1]Department of Chemistry, University of Warwick, Coventry, CV4 7AL, United Kingdom

[2]Laboratorio de Espectroscopía Atómica y Molecular (LEAM), Universidad Industrial de Santander. Bucaramanga, 678, Colombia

[3]Centro de Materiales y Nanociencias (CMN), Universidad Industrial de Santander, Bucaramanga, 678, Colombia

[4]Instituto Colombiano del Petróleo (ICP-Ecopetrol), Piedecuesta, Colombia

[5]Molecular Analytical Science Centre of Doctoral Training, University of Warwick, Coventry, CV4 7AL, United Kingdom

Abstract

In this work, a detailed analysis of a bio-oil obtained by pyrolysis of softwoods and its esterified product is described. Information of the type of chemical function groups were obtained by ^{13}C and ^{1}H nuclear magnetic resonance (NMR) and Fourier transform infrared spectroscopy (FT-IR) and compositional analysis was obtained by Fourier transform ion cyclotron resonance mass spectrometry (FTICR MS). The results obtained indicate that aliphatic hydrogen and carbon atoms are found in higher abundance, compared with aromatic hydrogen-carbon frameworks. Furthermore, a decrease in oxygen functional groups was observed after esterification. According to the FTICR MS results, the samples contain highly oxygenated species corresponding to compound classes O_x, NO_x and BO_x, with a high predominance of O_x species. After esterification, the compositions shifted towards lower oxygen-content, lower number of rings and double bonds, and longer alkyl chains as a consequence of the water removal via the condensation reaction.

Keywords: ultrahigh resolution mass spectrometry, pyrolysis, esterification, bio-oils, spectroscopy

1. Introduction

With energy demand projected to double by 2025 [1], the depletion of reserves of crude oil [2], and governmental policy changes with respect to the environment [3], it has been necessary to develop new and sustainable sources of energy [4]. Among

these, biodegradable organic matter, known as biomass, is playing an important role in the production of fuels and other chemical products. The conversion of biomass into fuel requires processes that vary depending upon the nature of the feedstock.

Biomass-derived fuels can be generated from lignocellulosic materials, such as softwood, agricultural residues, agricultural and municipal waste [5]. These materials contains three major building blocks: cellulose, hemicellulose and lignin [6]. Fast pyrolysis is a common method for processing lignocellulosic materials to generate bio-crude [7], a primary material and precursor of fuels. During this process, a biomass source is heated at a rate of over 100 K/s [8], and the vapours are rapidly condensed [9]. A dense liquid, often known as “tar” [10–12], is obtained in yields up to 70%. This liquid is a complex mixture of oxygenated and non-oxygenated hydrocarbons with properties including low calorific value, molecular weight greater than benzene, high oxygen and water content, low pH, high viscosity, low stability, and immiscibility with crude oil or other petroleum-derived resources [11,13,14].

To improve the properties of bio-oils and to use them for industrial production of higher value-added products, it is necessary to decrease the oxygen content within the samples after pyrolysis [10,15,16]. A widely applied methodology for upgrading bio-oils is known as esterification [15,17]. The esterification mechanism consists of the conversion of carboxylic acids to esters, using an excess of an alcohol in an acidic medium [18]. This significantly reduces the water content (upgrading) and conversely reduces the oxygen content [16].

To improve the energy content of biomass resources, a better knowledge of the biomass composition before and after processing is required. In previous studies, various analytical techniques have been utilized to characterize bio-oils, including mass spectrometry and spectroscopy [11,19]. Structural analysis of functional groups in bio-oils can be obtained by ^{1}H and ^{13}C nuclear magnetic resonance (NMR) spectroscopy [6,20,21]. Analogously, Fourier transform infrared spectroscopy (FT-IR) has been used to determine the functional groups present in bio-oils constituents [10,22–25]. Hence, spectroscopic techniques provide structural insight for the whole bio-oils compositions and are best suited to analyse changes in the functional group composition as a result of different upgrading processes. In parallel, ultrahigh resolution mass spectrometry has shown to be the state-of-the-art technique for the analysis of highly complex organic mixtures such as crude oils, vacuum residues, natural organic matter, and bio-oils [26–32]. In contrast to other analytical techniques, Fourier transform ion cyclotron resonance mass spectrometry (FTICR MS) affords unrivalled performance with respect to resolving power and mass accuracy; it is capable of resolving most of the small mass splits observed in complex samples and molecular formulae can be assigned to the tens of thousands of components in a single spectrum with a mass accuracy in the order of parts per billion (ppb) [33]. Therefore, a unique molecular formula can be assigned to each ionized species, and a detailed characterization of the complex sample becomes achievable. The characterization of pyrolysis bio-oil by petroleomics methods was reviewed by Martin Staš et. al. in 2017 [34].

In this work, the analysis of a bio-oil obtained by pyrolysis of Colombian softwood and its esterified product is presented, using ^{1}H and ^{13}C NMR, FT-IR, and FTICR

MS. The FTICR MS experiments were performed in conjunction with an atmospheric pressure photoionization (APPI) source operated in positive-ion mode for the characterization of non-polar components, and an electrospray ionization (ESI) source operated in both positive- and negative-ion mode.

2. Material and methods

2.1 Materials

A crude bio-oil was produced by fast pyrolysis using a mixture of softwoods (sample C) and the esterified product was obtained using a reactive distillation treatment with butanol in presence of H_2SO_4/dehydration (sample E).

A mixture of softwoods as raw material was used to produce a crude pyrolysis bio-oil with humidity less than 10% wt. Figure 1 shows a schematic of the pyrolysis pilot unit which consists of a fluidized bed reactor that operates at temperatures from 440°C to 500 °C. The lower part of the reactor has a preheated nitrogen inlet for provision of a carrier gas to ensure fluidization, while sand was used as a fluidizing medium. The coal produced in the thermal process was separated from the gas employing two cyclones in series. The condensation system consists of a column with trays which inject liquid bio-oil to assist the condensation of gases coming from the reactor, where this liquid bio-oil is kept in recirculation during the process. After this column, the system is completed with an electrostatic separator and a second condenser at 0 ° C to condense the lighter gases. The yield of crude pyrolysis bio-oil was 60% wt with respect to the biomass employed.

The crude pyrolysis bio-oil (sample C) was subjected to a reactive distillation treatment (a simultaneous process of esterification/dehydration) with n-butanol to reduce its acidity and deoxygenate it partially through water removal, producing the esterified bio-oil (sample E). n-butanol is useful in the simultaneous process, as it serves as a "water entraining agent" and in turn promotes esterification; this is due to the fact that this alcohol forms an azeotrope with a boiling temperature of 93 °C at 1 atmosphere of pressure. In this process, it is necessary to lower the boiling temperature to reduce the risk of thermal degradation of the bio-oil. Therefore, the system pressure was reduced to 250 mbar. For this system, the reaction was carried out in a rotary evaporator and the glass tube that connects the balloon containing the reaction mixture with the condenser was kept isolated to reduce heat losses and ensure that the vapors reached the condenser. To guarantee reflux conditions (at the boiling point of the azeotrope n-butanol: water), the butanol which was distilled (butanol phase) was periodically returned to the reaction vessel. The reaction time was five hours. The yield of esterified bio-oil was 68% wt with respect to the crude bio-oil sample.

2.2 Conventional analysis

The bulk properties of the samples were determined using the following methods: water content (ASTM E203); carbon residue using a standard test method for determination of carbon residue (ASTM D4530); density by means of a digital densimeter (ASTM D4052); viscosity (ASTM D445); weight percent of C, H, N and O by elemental analysis (ASTM D5291); high calorific value (ASTM D240); acid

number (ASTM standard D664); aromatic, phenolic or olefinic, and alkyl protons by ^{1}H NMR ^{13}C NMR; and FT-IR spectroscopy.

The ^{1}H and ^{13}C-NMR spectra of C and E samples were obtained using 400 MHz and 100 MHz Bruker Avance III NMR spectrometers (Bruker Biospin GMBH, Rheinstetten, Germany) instruments, respectively. 5% wt/wt solutions of MeOD were analyzed by ^{1}H NMR, with pulses of 30° obtained with 10 s of delay time (sweep width 6000 Hz). 32 scans were averaged for each spectrum and used for the statistical analysis. The ^{13}C NMR spectra were obtained with 30° pulses and a delay time of 20 s (sweep width 26000 Hz). The ^{13}C NMR samples were 10% solutions in MeOD. The phase and baseline of the resulting spectra were manually adjusted and corrected. The FT-IR spectra were acquired with an is50 FT-IR Nicolet (Thermo Scientific, Madison, USA) operating in the wavelength range of 4000-400 cm^{-1}, with a resolution of 4 cm^{-1}. A total of 32 scans were co-added during acquisition of each data set.

2.3 FTICR MS analysis

The samples were analysed with a 12 T solariX FTICR mass spectrometer (Bruker Daltonik GmbH, Bremen, Germany) coupled to an APPI ion source (positive-ion mode) and an Apollo II ESI ion source (positive- and negative-ion modes). The samples were diluted in toluene/methanol 50/50 % v/v solutions of toluene (HPLC grade 99.9%, Honeywell, Bracknell, UK) and methanol at 0.05 mg/mL. The solution was spiked with 0.5% of formic acid (98-100%, Merck, Feltham UK) prior to the

163 acquisition of positive-ion ESI mass spectra. Diluted samples were directly infused
164 using a flow rate of 300 μL/h and were accumulated for 0.060-0.350 seconds in the
165 collision cell prior to being transferred to the ICR cell for detection. The spectra were
166 acquired by co-adding 200 data sets using a detection range of m/z 100-2000 and a
167 4 MW data set size.

168

169 The mass spectra were externally calibrated using “ESI Tuning Mix” (Agilent
170 Technologies, Milton Keynes, UK), followed by internal recalibration with abundant
171 homologous alkylated compounds corresponding to O_4, O_3, and O_6 for both the
172 negative-ion ESI and positive-ion APPI data, and using homologous series of O_4[Na]
173 and O_6[Na] for the spectra acquired by ESI in positive-ion mode. A resolving power
174 of 520,000 FWHM at m/z 300 and mass accuracy <1ppm (RMS error of 0.43 ppm)
175 was achieved under the experimental condition described above. Composer version
176 1.5.7 (Sierra Analytics Inc., Modesto, CA, USA) was used to assign molecular
177 formulae to the thousands of components in each mass spectrum. Each ion was
178 assigned to a single elemental composition using the following constraints: maximum
179 of C_{200}, H_{1000}, N_3, S_1, O_{20}, B_1, Na_1, with a mass error below 1 ppm. The number of
180 rings plus double bonds (or double bond equivalents, DBE) for each elemental
181 formula, $C_cH_hN_nO_0B_b$, was calculated according to the following equation:

182

183 $$DBE = c - h/2 + n/2 + 1 \quad (1)$$

184

185 Where c, h and n are the numbers of carbon, hydrogen, and nitrogen atoms,
186 respectively. Each individual specie is then characterized by its heteroatomic class
187 $B_bN_nO_oS_s$, carbon number and DBE. Compound classes with the labels “[H]” and
188 “[Na]” denote protonated and sodium adducts, respectively, while those classes
189 without the label were observed as radical ions.

190

191 **3. Results and Discussion**

192

193 **3.1 Elemental analysis**

194

195 Biomass is composed of elemental C, H, O, N, S, and other heteroatoms, where 97-
196 99% of the compounds present correspond to compositions containing only carbon,
197 hydrogen, and oxygen; in general, higher carbon and hydrogen content results in a
198 higher calorific value of the biomass [35]. The conventional characterization of the
199 crude bio-oil and its esterified product (samples C and E, respectively) is given in
200 Table 1. The results from the conventional analyses show a significant improvement
201 of the quality of the product obtained after the reactive distillation (sample E). After
202 esterification, a decrease in the percent of water content, oxygen percent, acidity,
203 and density were observed, as well as an increase in the high calorific value and the
204 viscosity (at 40°C). Although the value of calorific content has increased from 16 to
205 30 MJ/kg, this value remains low compared with the average values reported for light
206 and heavy oils derived from petroleum (45 MJ/kg) [9]. The difference in energy
207 content can be explained in terms of the high oxygen content of both bio-oil samples;
208 an increase in oxygen content implies a limitation in the number of carbon and

209 hydrogen atoms in the compositions and, therefore, a decrease in the energy
210 content [36].

211

212 **3.2 Spectroscopic analysis**

213

214 The chemical environments of proton and carbon atoms can be characterized by ^{1}H
215 and ^{13}C NMR, respectively [6]. This allows, for example, the determination the
216 approximate aromatic-to-aliphatic ratios. To obtain high levels of accuracy for the ^{1}H
217 and ^{13}C NMR data, the phase, baseline, and integration were calculated. The
218 integrations were performed manually five times and the averaged results of the
219 areas for each chemical shift of ^{1}H and ^{13}C NMR data are shown in Table 2. The
220 chemical shift regions evaluated by ^{1}H NMR and ^{13}C NMR were based on values
221 from the literature [6,37].

222

223 After esterification ~56% of the protons corresponded to H_{alkyl} environments (CH_3 and
224 CH_2 from an aromatic ring), compared with only 8% of the protons in the same
225 region (0.5 - 1.6 ppm) in the original pyrolysis bio-oil (sample C). This demonstrates
226 that after esterification longer alkyl chains are found, which is in accordance with the
227 higher calorific value of this sample (see Table 1). In contrast, aliphatic protons
228 adjacent to aromatics or olefins or near to heteroatoms (2.0 - 3.3 ppm), were found
229 in higher relative abundance in the pyrolysis oil than the esterified product. The
230 increased alkyl chain lengths after esterification (region 0.5 – 1.0 ppm) explains the
231 reduction of the proportion of aliphatic protons CH3α, CH2α and CHα to an aromatic

232 ring after esterification. Protons in the region between 3.3 and 4.5 ppm correspond to
233 methylene groups, a moiety obtained after partial decomposition of lignin, aliphatic
234 alcohols, or ether, where similar environments were observed for both samples. By
235 contrast, $H_{phenolics}$ or $H_{olefinics}$ and $H_{aromatic}$ were predominant in the pyrolysis sample,
236 indicating that sample C contains more aromatic moieties and carbohydrate-like
237 molecules.

238

239 Similar results were found by ^{13}C NMR. As shown in **Error! Reference source not**
240 **found.**, carbon atoms in the region 28-55 ppm, corresponding to long and branched
241 aliphatic chains, are found in higher abundance after esterification, while carbon
242 atoms correlated with carbohydrate-like structures, alcohols, phenols, methoxys, and
243 sugars are predominant in the pyrolysis sample. The region corresponding to
244 aromatic and olefinic carbon atoms (95 - 165 ppm) differs noticeably between the
245 samples. The ^{13}C NMR data suggests that sample C contains a higher proportion of
246 carbon atoms in aromatic (95 - 165 ppm), carboxylic acid and esters (165 - 180 ppm)
247 and ketones/aldehyde environments (180 - 215 ppm). The significant overlap of
248 signals of the NMR shifts causes ambiguous assignments of the different functional
249 groups [20]. For instance, the signals between 165 - 180 ppm can be assigned to
250 both carboxylic acid and esters functional groups. Due to such overlaps, it is not
251 possible to assure the specific value for each contribution. However, considering that
252 the mechanism of acid catalysed esterification with alcohols is well established
253 [38,39], and the considerable reduction of the total acid number of the sample E (see
254 Table 1), the reduction of this signal can be due to the esterification of carboxylic
255 acids compositions within the pyrolysis bio-oil.

256 The FT-IR spectra for bio-oil samples (Fig. 2) provide information about the
257 functional groups, with characteristic absorption bands in the mid-IR [11]. The typical
258 functional groups that can be assigned from the IR signal are shown in Table 3 [40].
259 The first broad band at 3000 - 3700 cm^{-1} corresponds to O–H stretching vibration in
260 phenols, alcohols, carboxylic acids, and water. The vibration modes observed
261 between 2958 cm^{-1} and 2873 cm^{-1} are associated with aliphatic C–H stretching
262 vibrations, which has higher intensity in the esterified sample, corroborating the
263 results obtained by NMR. As can be seen in Fig. 2, the lower water content (due to
264 the condensation reaction as part of the esterification process) and acidity after
265 esterification correlate with the decreased O–H stretching vibration and the increase
266 of the aliphatic C–H bands. These observations are in line with the other results,
267 including the decrease in oxygen percent, density, water content, phenolic fraction
268 (^{1}H NMR), carbohydrate fraction (^{13}C NMR), and the increase of the high calorific
269 content. The reduction of the carboxylic acid contribution after esterification is
270 exemplified by the lower intensity of the bands at 1613 cm^{-1} and at 3000-3700 cm^{-1},
271 in addition to the lower acidity of the sample.

272

273 The higher intensity of the bands at 1112 cm^{-1} and 1243 cm^{-1} show the increase of
274 esters in the upgraded product, sample E. Additionally, a lower intensity of the band
275 corresponding to C=C aromatic (band at 1613 cm^{-1}) was observed for sample E and,
276 thus, a decrease in aromaticity after esterification, which is in line with the findings
277 from the NMR data. Esterification also resulted in a higher contribution of C–O
278 stretching from saturated aliphatic primary alcohols, esters, ethers and acids (1000
279 and 1100 cm^{-1})[11], possibly due to remaining n-butanol or the formation of esters.

The alcohol serves as a "water entraining agent" and promotes esterification, as it forms an azeotrope with a boiling temperature of 93 ºC at 1 atmosphere of pressure). Based on the change in the peak height at 1613 cm^{-1} and the vibration modes observed between 1112 cm^{-1}, and 1029 cm^{-1}, a decrease of the C=C aromatic environments was observed, as well as increase of C–O–C symmetric and asymmetric stretching, C–O stretching, saturated aliphatic primary alcohols after esterification. A decrease of the band corresponding to C=C indicated the formation of acetals after the esterification of aldehydes. According to these results, good agreement was observed between the structural analyses obtained by NMR, FT-IR, and the elemental analysis shown in **Error! Reference source not found.**.

3.3 FTICR MS

FTICR MS can be coupled to different ionization sources, where each ionization source provides complementary information of the composition of the sample. For example, APPI ionizes non-polar compounds such as polycyclic aromatic compounds (PAHs) and polycyclic aromatic sulfur heterocycles (PASHs), in addition to being suitable for ionization of non/low- polar lipids [41], aromatic carboxylic acids, ketones, lactones and some alcohols [42]. On the other hand, ESI preferentially ionizes a wide range of polar compounds, such as basic species in positive-ion mode and acidic compounds in negative-ion mode. The differences in ionization can be utilized to gain greater insight into sample compositions. APPI offers advantages with respect to ionization of a broader range of organic compounds, while the

303 selectivity of ESI can be used to differentiate between acidic and basic components,
304 for example.

305

306 The ultrahigh resolution and high mass accuracy provided by FTICR mass
307 spectrometry affords the ability to assign a unique molecular formula for each
308 detected ion. In ultrahigh resolution mass spectra of petroleum-related samples,
309 series with an exact mass difference of 14.01565 Da can be observed. These series
310 correspond to ions differing by multiples of CH_2 units (alkylation series) with the
311 same heteroatomic class and DBE. The series can be categorized by class with a
312 general formula $C_cH_hN_nO_oS_sB_b$. With these capabilities, thousands of species were
313 detected within a mass range of m/z 200-800, see Fig. 3. A total of 3427 and 4019
314 species were identified by ESI in negative-ion mode for samples C and E,
315 respectively. Also, 2390 and 5315 species were detected by electrospray in positive-
316 ion mode (samples C and E, respectively). APPI ionizes the broadest range of
317 components, leading to the assignment of approximately 6100 compositions
318 including both radical and protonated compositions.

319

320 The pyrolysis bio-oil and its esterified product are characterized by a broad range of
321 oxygen-containing species, as shown by the range of oxygen-containing compound
322 classes in Fig. 4, observed using negative-ion and positive-ion ESI, as well as
323 positive-ion APPI. Furthermore, Fig. 4 provides the DBE vs. carbon number plots of
324 selected compound classes, one corresponding to organic species with 5 oxygen
325 atoms (O_5[H] class) and other with 12 oxygen atoms (O_{12}[H] class). In positive-ion
326 mode ESI, O_x[Na] compositions (x= 3-16) were predominantly detected and a shift of

327 the relative abundance of lower oxygen-containing species is observed after
328 esterification. The formation of sodium adduct ions in known to occur due to the
329 presence of trace amounts of impurities in solvents, glassware, or the formic acid
330 introduced for the sample treatment [34,43,44].

331

332 The species ionized by ESI in negative-ion mode correspond to polyoxygenated
333 compounds containing hydroxyl or carboxylic acids groups [42,45]. Thus,
334 compounds classes such as ketones, furans and methylphenols (with relative low
335 response), methoxyphenols, dimethoxyphenols and carboxylic acids such as valeric
336 acid, trimesic acid, biphenyl-4-carboxyl acid, among others can be ionized by
337 negative-ion ESI [44,46]. As shown in Fig. 4, the acidic species detected by
338 negative-ion ESI are dominated by the oxygenated compound classes $O_2 - O_{17}$, with
339 a shift towards lower oxygen-containing species after esterification. Along with O_x
340 species, BO_x (O_6 - O_{12}) compositions were observed in the samples and these
341 assignments were supported by the isotopic pattern information. Boron is an
342 essential micronutrient found in higher plants [47], and has been previously detected
343 in pyrolyzed bio-oils by FTICR MS in 2014 by Jarvis et. al [48].

344

345 As shown in Fig. 5 (and Fig. S4 in the supplementary data), the compositions with
346 higher oxygen-containing species ($O_{x>7}$[H]) demonstrated a shift towards higher
347 carbon number after esterification, which indicated a longer alkyl chain of the
348 esterified molecules. Furthermore, a general trend towards lower DBE is observed
349 by class after esterification (see Fig. 5 and Fig. S5). In particular, an increased in the
350 relative abundance of species with DBE 1, 2, 3 and 4 is observed in some classes

e.g. O_2[H], O_7[H], O_{10}[H], O_{14}[H] respectively. This indicates the formation of acetals from the reaction with aldehyde groups, rather than carboxylic acid groups, within the compositions. These findings are consistent with the data obtained by elemental analysis, NMR, and FT-IR, and indicate side reactions in addition to the intended esterification.

Non-polar compounds, such as PAHs and PASHs, and a number of polar species can be detected by APPI. Additionally, species containing alcohols, aldehydes, ketones, carboxylic acids and cyclic carboxylic acids functional groups can also be detected by APPI [42]. According to Fig. 4, the hydrocarbon compounds not containing a heteroatom had a relative abundance of approximately 2%, while oxygen-containing compounds, detected as protonated species and radical ions, were detected in greater relative abundance. For a given compound class, there is a distribution of compounds with respect to both double bond equivalents with alkyl length (number of carbon atoms); this is typically represented in DBE versus carbon number plots. Decreasing the number of hydrogen atoms in a molecule (i.e. increasing double bonds and/or rings in a molecule) increases the DBE and hence the degree of unsaturation [49]. The DBE is therefore related to the number of carbon, hydrogen, and nitrogen atoms, but is independent of the number of oxygen and sulfur atoms (see Equation 1). Thus, species with DBE = 0 correspond to molecules containing single bonds, species with DBE = 1 can contain one double bond between two carbon atoms or a double bond between one carbon atom and a heteroatom such as oxygen (see Equation 1) or include a single ring, and so forth. For a six-membered aromatic ring to be present, the molecule must have a DBE ≥ 4

375 in its neutral form or as a radical ion (≥3.5 for protonated species in positive-ion
376 mode, ≥4.5 for deprotonated species in negative-ion mode).

377

378 Double bond equivalents versus carbon number plots of O_5[H] and O_{12}[H] compound
379 classes, obtained by negative-ion ESI of sample C and E can be found in the bottom
380 right of Fig. 4 (DBE plots of O_x classes where x= 2 – 15 are shown in Fig. S3).
381 Species with five oxygen atoms had a DBE range between 2 and 14, with a higher
382 relative abundance of species with lower DBE after esterification. Species with 12
383 oxygen atoms had DBE ranges of 2-19 and 2-16 for samples C and E, respectively.
384 Species with a high oxygen content and low DBE (e.g $C_{10}H_{18}O_{10}$, 0.136 ppm
385 corresponding to a component with DBE = 2) potentially indicated the presence of
386 alcohols and ethers within the molecular structure, as including more than one
387 functional group corresponding to ketones, aldehydes, or carboxylic acids groups
388 would increase the number of double bonds, and hence, the DBE value. In similarity
389 with the results obtained by NMR and IR, the analysis and the DBE plots that can be
390 obtained from ultrahigh resolution FTICR MS data clearly show that the species
391 contain higher numbers of carbon atoms after esterification, an indication of increase
392 of alkylation during the formation of esters and acetals, for example, as expected
393 after esterification [38]. For the addition of a butyl chain, resulting from the use of n-
394 butanol during esterification, the carbon number would be expected to increase by 4
395 per ester formed or by 8 per acetal formed, for example. In petroleum samples, a
396 high DBE is normally associated with the high aromaticity of the hydrocarbon
397 components. The low percentage of aromatic carbon atoms observed by ^{13}C-NMR
398 and FT-IR and the high relative abundance of highly oxygen-containing species
399 identified by FTICR MS, however, indicate that the species in samples C and E with

high DBE can incorporate oxygen atoms in functional groups corresponding to carboxylic acids, aldehydes, or ketones rather than aromatic rings. The acetalization of aldehydes and ketones in presence of alcohols during esterification can explain the shift towards lower DBEs of the classes detected in sample E. Thus, after esterification, organic species containing oxygen (categorized as O_x and NO_x, compound classes) have higher relative abundance of species with lower DBEs and higher carbon number.

4. Conclusions

A pyrolysis bio-oil and its esterified product were analysed. The NMR and FT-IR data showed an increase of the total aliphatic content after esterification and a low abundance of aromatic moieties in both samples. The species detected by FTICR MS correspond to classes with high oxygen content (O_2-O_{17}), in addition to compound classes incorporating other heteroatoms (e.g. NO_x and BO_x) with up to 40 carbon atoms and a maximum of 20 rings and double bonds within their structures. The elemental compositions with low DBE and high oxygen content indicate the presence of alcohols and ethers within the molecular structure.

Supplementary material

E-supplementary data of this work can be found in online version of the paper.

Acknowledgments

This work was supported by a Newton Fund award (reference number 275910721), Research Agreement No. 5211770 UIS-ICP, COLCIENCIAS (project No. N° FP44842496-2016), and by the Engineering and Physical Sciences Research Council (EPSRC) for the Centre for Doctoral Training in Molecular Analytical Science (grant number EP/L015307/1). The authors would also like to thank David Stranz (Sierra Analytics, Modesto, CA, USA) for additional development of Composer and useful discussions.

Declaration of Interest

Declarations of interest: none

References

[1] Ragauskas AJ, Williams CK, Davison BH, Britovsek G, Cairney J, Eckert CA, et al. The Path Forward for Biofuels and Biomaterials. Science (802006;311:484–9. doi:10.1126/science.1114736.

[2] Charry-Sanchez J, Betancourt-Torcat A, Almansoori A. Environmental and Economics Trade-Offs for the Optimal Design of a Bitumen Upgrading Plant. Ind Eng Chem Res 2016;55:11996–2013. doi:10.1021/acs.iecr.6b01145.

[3] Wallace D. Environmental policy and industrial innovation: Strategies in Europe, the USA and Japan. 1st Editio. London: Routledge; 2017.

[4] Shylesh S, Gokhale AA, Ho CR, Bell AT. Novel Strategies for the Production of Fuels, Lubricants, and Chemicals from Biomass. Acc Chem Res 2017;50:2589–97. doi:10.1021/acs.accounts.7b00354.

[5] Abdelnur P V., Vaz BG, Rocha JD, De Almeida MBB, Teixeira MAG, Pereira

RCL. Characterization of bio-oils from different pyrolysis process steps and biomass using high-resolution mass spectrometry. Energy and Fuels 2013;27:6646–54. doi:10.1021/ef400788v.

[6] Mullen CA, Strahan GD, Boateng AA. Characterization of various fast-pyrolysis bio-oils by NMR spectroscopy. Energy and Fuels 2009;23:2707–18. doi:10.1021/ef801048b.

[7] Carpenter D, Westover TL, Czernik S, Jablonski W. Biomass feedstocks for renewable fuel production: A review of the impacts of feedstock and pretreatment on the yield and product distribution of fast pyrolysis bio-oils and vapors. Green Chem 2014;16:384–406. doi:10.1039/c3gc41631c.

[8] Liu Y, Li Z, Leahy JJ, Kwapinski W. Catalytically upgrading bio-oil via esterification. Energy and Fuels 2015;29:3691–8. doi:10.1021/acs.energyfuels.5b00163.

[9] Mohan D, Pittman CU, Steele PH. Pyrolysis of wood/biomass for bio-oil: A critical review. Energy and Fuels 2006;20:848–89. doi:10.1021/ef0502397.

[10] Volpe M, Panno D, Volpe R, Messineo A. Upgrade of citrus waste as a biofuel via slow pyrolysis. J Anal Appl Pyrolysis 2015;115:66–76. doi:10.1016/j.jaap.2015.06.015.

[11] Kanaujia PK, Sharma YK, Agrawal UC, Garg MO. Analytical approaches to characterizing pyrolysis oil from biomass. TrAC - Trends Anal Chem 2013;42:125–36. doi:10.1016/j.trac.2012.09.009.

[12] A. Milne T, Abatzaglou N, Evans R. Biomass Gasifier Tars : Their Nature, Formation, and Conversion 1998.

[13] Si Z, Zhang X, Wang C, Ma L, Dong R. An Overview on Catalytic Hydrodeoxygenation of Pyrolysis Oil and Its Model Compounds. Catalysts 2017;7:169–91. doi:10.3390/catal7060169.

[14] Talmadge MS, Baldwin RM, Biddy MJ, McCormick RL, Beckham GT, Ferguson GA, et al. A perspective on oxygenated species in the refinery integration of pyrolysis oil. Green Chem 2014;16:407–53. doi:10.1039/c3gc41951g.

[15] Xu J, Jiang J, Dai W, Zhang T, Xu Y. Bio-oil upgrading by means of ozone oxidation and esterification to remove water and to improve fuel characteristics. Energy and Fuels 2011;25:1798–801. doi:10.1021/ef101726g.

[16] Hu X, Gunawan R, Mourant D, Hasan MDM, Wu L, Song Y, et al. Upgrading of bio-oil via acid-catalyzed reactions in alcohols — A mini review. Fuel Process Technol 2017;155:2–19. doi:10.1016/j.fuproc.2016.08.020.

[17] Wang JJ, Chang J, Fan J. Upgrading of bio-oil by catalytic esterification and determination of acid number for evaluating esterification degree. Energy and Fuels 2010;24:3251–5. doi:10.1021/ef1000634.

[18] Vančik H. Basic organic chemistry for the life sciences. vol. 52. Switzerland: Springer International Publishing; 2015. doi:10.1007/978-3-319-07605-8.

[19] Volpe M, D'Anna C, Messineo S, Volpe R, Messineo A. Sustainable production of bio-combustibles from pyrolysis of agro-industrial wastes. Sustain 2014;6:7866–82. doi:10.3390/su6117866.

[20] Hao N, Ben H, Yoo CG, Adhikari S, Ragauskas AJ. Review of NMR Characterization of Pyrolysis Oils. Energy and Fuels 2016;30:6863–80.

492 doi:10.1021/acs.energyfuels.6b01002.

493 [21] Tessarolo NS, Silva RVS, Vanini G, Casilli A, Ximenes VL, Mendes FL, et al.
494 Characterization of thermal and catalytic pyrolysis bio-oils by high-resolution
495 techniques:1H NMR, GC × GC-TOFMS and FTICR MS. J Anal Appl Pyrolysis
496 2016;117:257–67. doi:10.1016/j.jaap.2015.11.007.

497 [22] Junming X, Jianchun J, Yunjuan S, Yanju L. Bio-oil upgrading by means of
498 ethyl ester production in reactive distillation to remove water and to improve
499 storage and fuel characteristics. Biomass and Bioenergy 2008;32:1056–61.
500 doi:10.1016/j.biombioe.2008.02.002.

501 [23] Kostyukevich Y, Vlaskin M, Borisova L, Zherebker A, Perminova I, Kononikhin
502 A, et al. Investigation of bio-oil produced by hydrothermal liquefaction of food
503 waste using ultrahigh resolution Fourier transform ion cyclotron resonance
504 mass spectrometry. Eur J Mass Spectrom 2017:1–8.

505 [24] Santos RM, Santos AO, Sussuchi EM, Nascimento JS, Lima ÁS, Freitas LS.
506 Pyrolysis of mangaba seed: Production and characterization of bio-oil.
507 Bioresour Technol 2015;196:43–8. doi:10.1016/j.biortech.2015.07.060.

508 [25] Agrawalla A, Kumar S, Singh RK. Pyrolysis of groundnut de-oiled cake and
509 characterization of the liquid product. Bioresour Technol 2011;102:10711–6.
510 doi:10.1016/j.biortech.2011.08.113.

511 [26] Barrow MP. Petroleomics: study of the old and the new. Biofuels 2010;1:651–
512 5. doi:10.4155/bfs.10.55.

513 [27] Headley J V, Barrow MP, Fahlman B, Frank RA, Bickerton G. Preliminary
514 fingerprinting of Athabasca oil sands polar organics in environmental samples

using electrospray ionization Fourier transform ion cyclotron resonance mass spectrometry. Rapid Commun Mass Spectrom 2011;25:1899–909. doi:10.1002/rcm.5062.

[28] Shi Q, Hou D, Chung KH, Xu C, Zhao S, Zhang Y. Characterization of heteroatom compounds in a crude oil and its saturates, aromatics, resins, and asphaltenes (SARA) and non-basic nitrogen fractions analyzed by negative-ion electrospray ionization fourier transform ion cyclotron resonance mass spectrome. Energy and Fuels 2010;24:2545–53. doi:10.1021/ef901564e.

[29] Palacio Lozano DC, Orrego-Ruiz JA, Barrow MP, Cabanzo Hernandez R, Mejía-Ospino E. Analysis of the molecular weight distribution of vacuum residues and their molecular distillation fractions by laser desorption ionization mass spectrometry. Fuel 2016;171:247–52. doi:10.1016/j.fuel.2015.12.058.

[30] Ramírez CX, Torres JE, Catalina D, Lozano P, Arenas-Diaz JP, Mejia-ospino E, et al. Molecular Representation of Molecular Distillation Cuts of Vacuum Residue by Spectrometry Ultra-High Resolution and Conventional Analytic. Chem Eng Trans 2017;57:1069–74. doi:10.3303/CET1757179.

[31] Bouslimani A, Sanchez LM, Garg N, Dorrestein PC. Mass spectrometry of natural products: current, emerging and future technologies. Nat Prod Rep 2014;31:718–29. doi:10.1039/c4np00044g.

[32] Reemtsma T. Determination of molecular formulas of natural organic matter molecules by (ultra-) high-resolution mass spectrometry. Status and needs. J Chromatogr A 2009;1216:3687–701. doi:10.1016/j.chroma.2009.02.033.

[33] Hsu CS. Mass resolving power requirement for molecular formula determination of fossil oils. Energy and Fuels 2012;26:1169–77.

539 doi:10.1021/ef201848k.

540 [34] Staš M, Chudoba J, Kubicka D, Blazek J, Pospíšil M. Petroleomic
541 Characterization of Pyrolysis Bio-oils: A Review. Energy & Fuels
542 2017;31:10283–99. doi:10.1021/acs.energyfuels.7b00826.

543 [35] Sheng C, Azevedo JLT. Estimating the higher heating value of biomass fuels
544 from basic analysis data. Biomass and Bioenergy 2005;28:499–507.
545 doi:10.1016/j.biombioe.2004.11.008.

546 [36] Kim S, Kramer RW, Hatcher PG. Graphical Method for Analysis of Ultrahigh-
547 Resolution Braodband mass spectra of Natural Organic Matter, the Van
548 Krevelen diagram. Anal Chem 2003;75:5336–44. doi:10.1021/ac034415p.

549 [37] Qing W, Chunxia J, Jianxin G, Wenxue G. 1H NMR and 13 C NMR Studies of
550 Oil from Pyrolysis of Indonesian Oil Sands. Energy and Fuels 2016;30:2478–
551 91. doi:10.1021/acs.energyfuels.5b01215.

552 [38] Sundqvist T, Oasmaa A, Koskinen A. Upgrading fast pyrolysis bio-oil quality by
553 esterification and azeotropic water removal. Energy and Fuels 2015;29:2527–
554 34. doi:10.1021/acs.energyfuels.5b00238.

555 [39] Ciddor L, Bennett JA, Hunns JA, Wilson K, Lee AF. Catalytic upgrading of bio-
556 oils by esterification. J Chem Technol Biotechnol 2015;90:780–95.
557 doi:10.1002/jctb.4662.

558 [40] Socrates G. Infrared and Raman characteristic group frequencies. Third edit.
559 John Wiley & Sons Ltd; 2004.

560 [41] Awad H, Khamis MM, El-Aneed A. Mass spectrometry, review of the basics:
561 Ionization. Appl Spectrosc Rev 2015;50:158–75.

562 doi:10.1080/05704928.2014.954046.

563 [42] Katarina A, Huba K, Gardinali PR. Understanding the atmospheric pressure
564 ionization of petroleum components: The effects of size, structure, and
565 presence of heteroatoms. Sci Total Environ 2016;563–564:600–10.
566 doi:10.1016/j.scitotenv.2016.06.044.

567 [43] Andrianova AA, DiProspero T, Geib C, Smoliakova IP, Kozliak EI, Kubátová A.
568 Electrospray Ionization with High-Resolution Mass Spectrometry as a Tool for
569 Lignomics: Lignin Mass Spectrum Deconvolution. J Am Soc Mass Spectrom
570 2018;29:1044–59. doi:10.1007/s13361-018-1916-z.

571 [44] Staš M, Chudoba J, Auersvald M, Kubička D, Conrad S, Schulzke T, et al.
572 Application of orbitrap mass spectrometry for analysis of model bio-oil
573 compounds and fast pyrolysis bio-oils from different biomass sources. J Anal
574 Appl Pyrolysis 2017;124:230–8. doi:10.1016/j.jaap.2017.02.002.

575 [45] Tessarolo NS, dos Santos LRM, Silva RSF, Azevedo DA. Chemical
576 characterization of bio-oils using comprehensive two-dimensional gas
577 chromatography with time-of-flight mass spectrometry. J Chromatogr A
578 2013;1279:68–75. doi:10.1016/j.chroma.2012.12.052.

579 [46] Peru KM, Thomas MJ, Palacio Lozano DC, McMartin DW, Headley J V.,
580 Barrow MP. Characterization of oil sands naphthenic acids by negative-ion
581 electrospray ionization mass spectrometry: Influence of acidic versus basic
582 transfer solvent. Chemosphere 2019;222:1017–24.
583 doi:10.1016/j.chemosphere.2019.01.162.

584 [47] Hu H, Penn SG, Lebrilla CB, Brown PH. Isolation and Characterization of
585 Soluble Boron Complexes in Higher Plants (The Mechanism of Phloem

586 Mobility of Boron). Plant Physiol 1997;113:649–55. doi:10.1104/pp.113.2.649.

587 [48] Jarvis JM, Page-dumroese DS, Anderson NM, Corilo Y, Rodgers RP.
588 Characterization of Fast Pyrolysis Products Generated from Several Western
589 USA woody species. Energy and Fuels 2014;28:6438–46.

590 [49] Koch BP, Dittmar T. From mass to structure: An aromaticity index for high-
591 resolution mass data of natural organic matter. Rapid Commun Mass
592 Spectrom 2006;20:926–32. doi:10.1002/rcm.2386.

593

594 Figure:

595 Fig. 1. Schematic diagram of the pyrolysis of the biomass.

596 Fig. 2. FT-IR spectra of the bio-oil (sample C) and its esterified product (sample E).

597 Fig. 3. Negative-ion mode ESI FTICR MS of the bio-oil (C) and its esterified product
598 (E). The insets show an expanded region of 0.32 Da with selected assignments.

599 Fig. 4. Class distribution obtained by positive- and negative-ion mode ESI (labelled
600 ESI(+) and ESI(-), respectively) and positive-ion APPI (labelled APPI(+)) of samples
601 C and E. The graphs in the bottom right show a comparison of the double bond
602 equivalents versus carbon number plots of the O5[H] and O12[H] compound classes
603 from the negative-ion ESI data.

604 Fig. 5. Relative abundance of the carbon number and DBE distribution for classes
605 O5[H] and O12[H] detected by negative-ion mode ESI. Species with higher oxygen-
606 content showed a shift toward higher carbon number after esterification.

607

608 **Table captions**

609 Table 1. Conventional analysis of the crude bio-oil, sample C, and its esterified
610 product, sample E.

611

612 Table 2. 13C and 1H NMR of the pyrolysis bio-oil (samples C) and its esterified
613 product (sample E). The standard deviation is 0.25 - 1.43.

614

615 Table 3. Assignments of the FT-IR bands of the bio-oil and its esterified product.

616

617

618

619

620

621

622

623

624

625

626

627

628

629

630 Figure 1

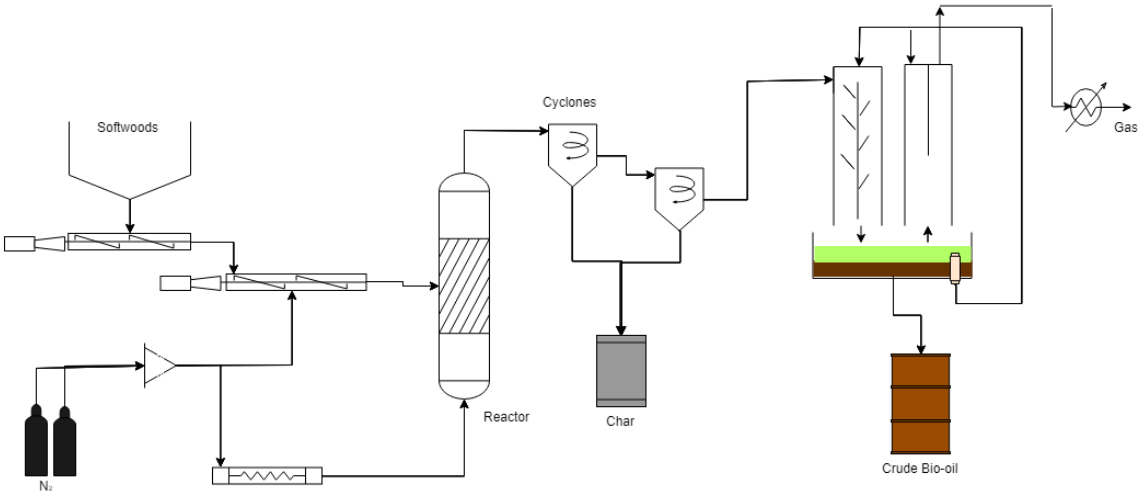

631

632

633

634

635

636

637

638

639

640

641

642

643

644 Figure 2

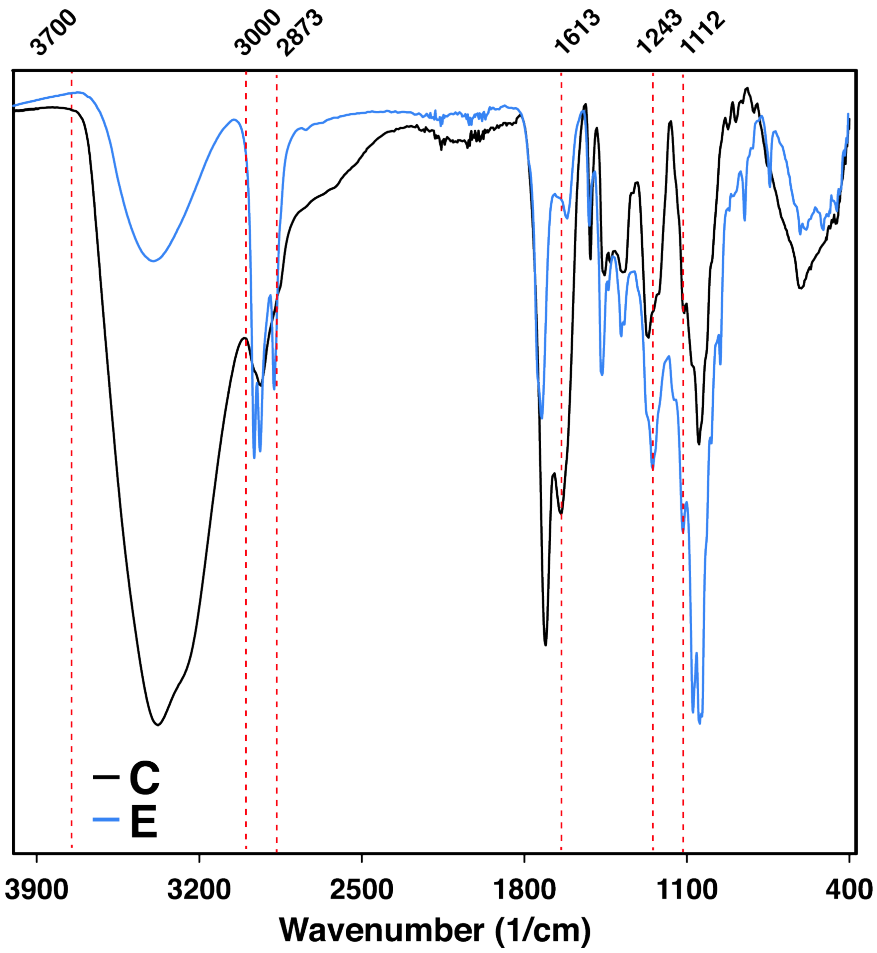

645

646

647

648

649

650

651

Figure 3

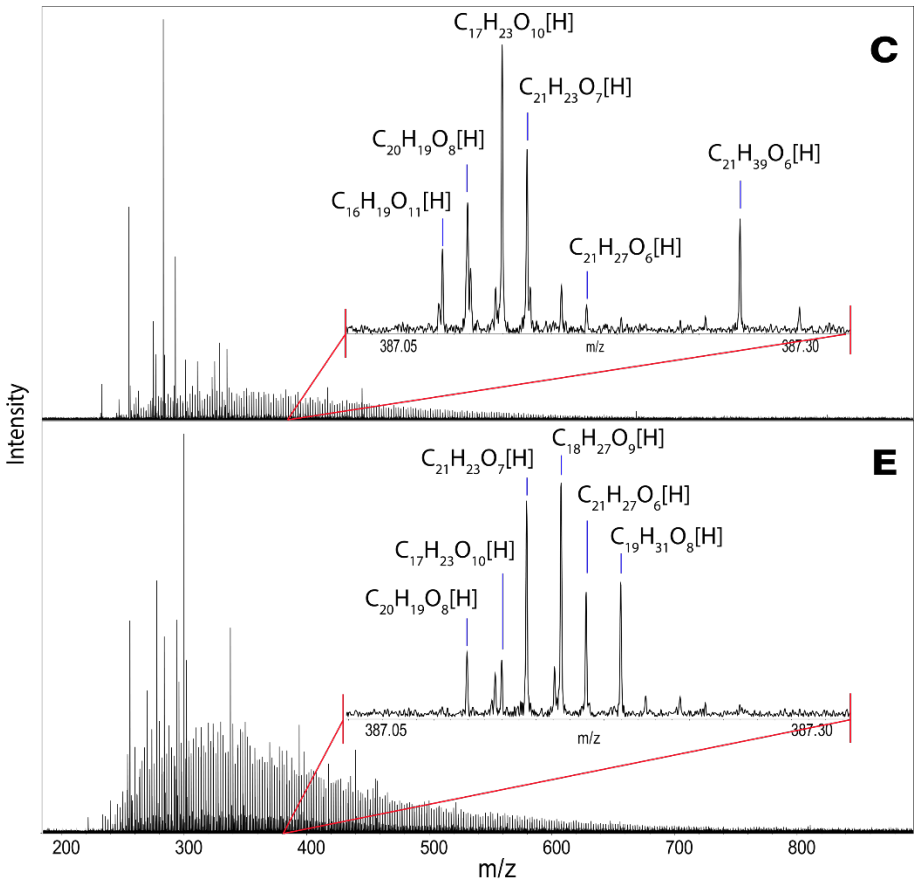
C
$C_{17}H_{23}O_{10}[H]$
$C_{21}H_{23}O_{7}[H]$
$C_{20}H_{19}O_{8}[H]$
$C_{21}H_{39}O_{6}[H]$
$C_{16}H_{19}O_{11}[H]$
$C_{21}H_{27}O_{6}[H]$
387.05
m/z
387.30
E
$C_{18}H_{27}O_{9}[H]$
$C_{21}H_{23}O_{7}[H]$
$C_{21}H_{27}O_{6}[H]$
$C_{19}H_{31}O_{8}[H]$
$C_{17}H_{23}O_{10}[H]$
$C_{20}H_{19}O_{8}[H]$
387.05
m/z
387.30
Intensity
200
300
400
500
600
700
800
m/z

659 Figure 4

660

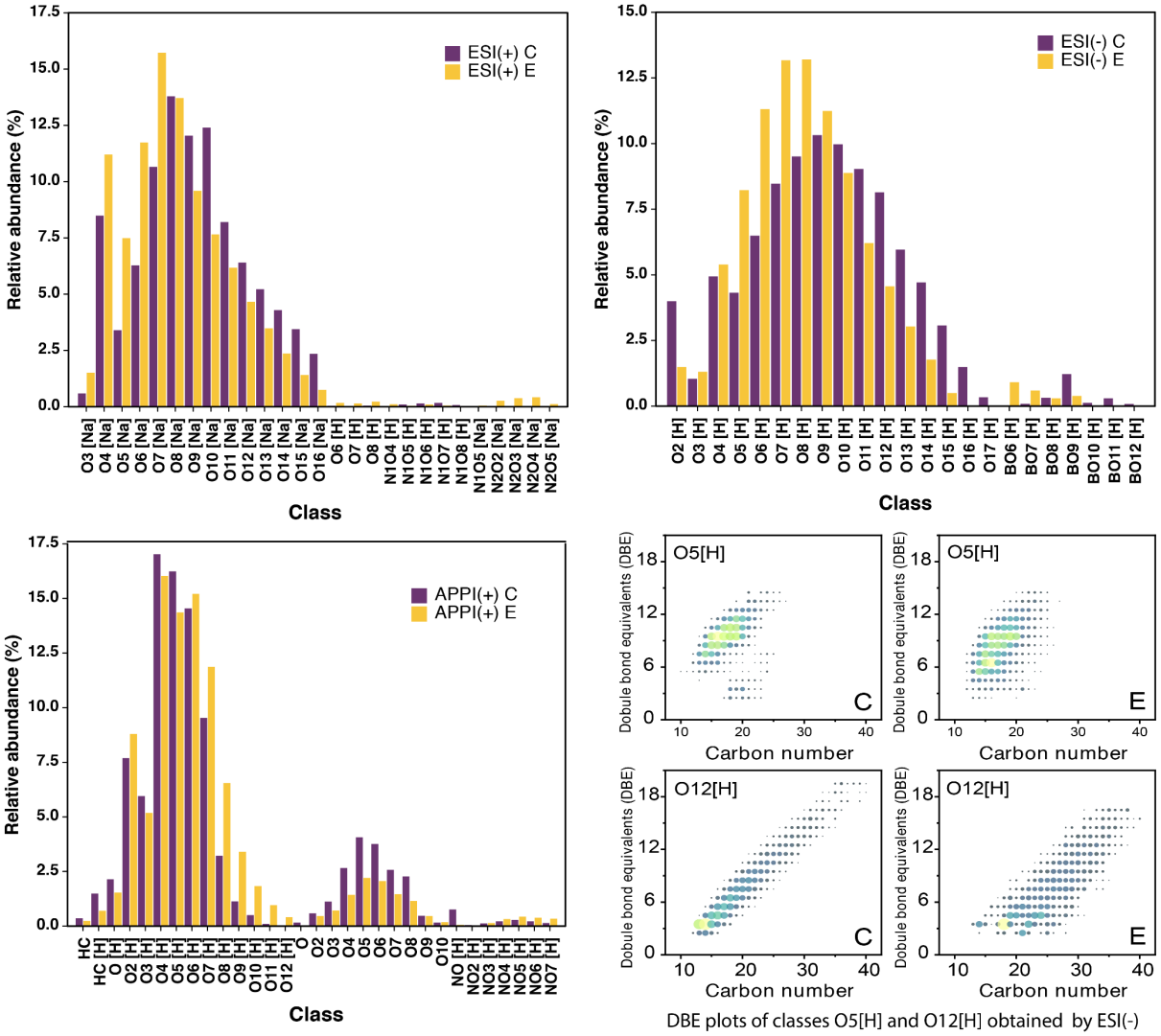

661 DBE plots of classes O5[H] and O12[H] obtained by ESI(-)

662

663

664

665

666

667

Figure 5

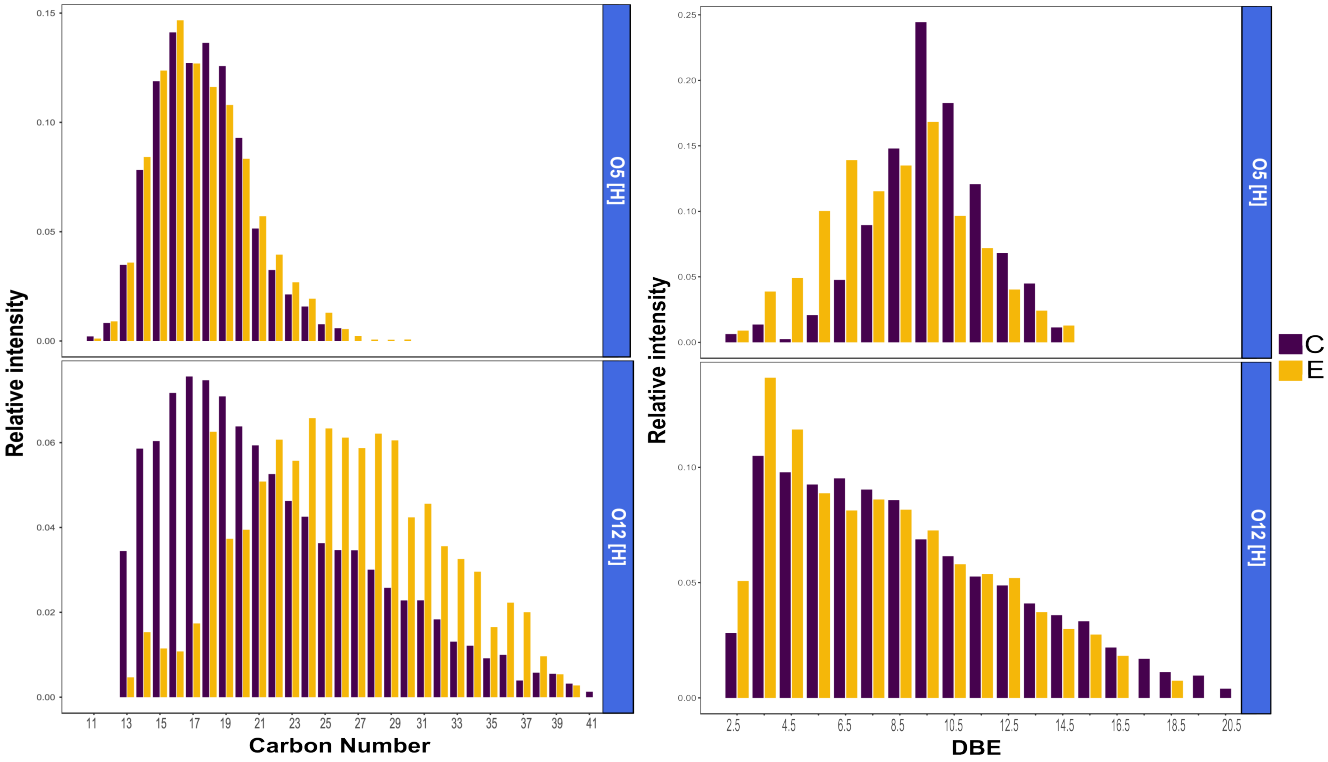

680 Table 1

Property	Sample	
	C	E
High calorific value (MJ/kg)	16	30
Density (g/mL)	1.206	1.043
Viscosity (40 °C) mm^2/s	23.4	37.1
Water content (wt%)	22.6	1.2
Total acid number (mg KOH/g)	214.9	62.5
Elemental composition		
C (% wt)	45.3	62.7
H (%wt)	8.9	10.6
N (%wt)	1.2	0.8
O*(%wt)	45.8	26

681 * Value obtained by difference

682

683

684

685

686

687

688

689

690

691

692 Table 2

Functional groups and structures	**Chemical shifts (ppm)**	**%C**	
		C	E
Ketones, aldehydes	180 - 215	11.3	8.0
Esters, carboxylic acids	165 - 180	9.3	5.0
Aromatics, olefins	95 - 165	32.7	25.6
Alcohols, ethers, phenolics, methoxys, carbohydrates, sugars	55 - 95	24.6	19.4
Long and branched aliphatics	28 - 55	13.1	17.0
Short aliphatics	0 - 28	9.0	24.9
Total aliphatics	0 - 55	22.1	41.9
Proton environment	**Chemical shifts (ppm)**	**%H**	
$H_{aromatic}$	6.5 - 9	8.7	2.1
$H_{phenolic/\ oleofin}$	5 – 6.5	33.7	2.2
$H_{ring\text{-}join\ methylene}$	3.3 – 4.5	25.2	27.5
H Alkyl CH3α, CH2α and CHα to an aromatic ring	2.0 – 3.3	19.7	7.0
H Alkyl CH2α, CHα to an α ring (naphtenic)	1.6 – 2	4.9	4.7
H Alkyl CH3β CH2β and, CHγ from an aromatic ring	1.0 – 1.6	6.7	32.3
H Alkyl CH3γ from an aromatic ring	0.5 - 1	1.1	24.3

693

694

695

696

697

698

699 Table 3

Functional group	**Wavenumber [cm^{-1}]**
O–H stretching	3000-3700
C–H asymmetric stretching, CH_3	2958
C–H asymmetric stretching, CH_3– aromatic, –CH_2– alkanes	2933
C–H symmetric stretching, CH_3, –CH_2– alkanes	2873
C=O stretching aryl esters, C=O stretching, saturated aliphatic carboxylic acids dimers	1720
N–H def primary amines, C=C stretching, aromatic –C=C–,	1613
C=C aromatic stretching	1515
–CH_2– scissoring alkanes, CH_3 asymmetric	1464
C–O stretching and OH deformation, carboxylic acids	1433
SO_2 asymmetric stretching, C–H symmetric deformation - CH_3	1378
C–O stretching	1366
C–O carboxylic acids dimers, C–O–C asymmetric stretching, saturated aliphatic esters	1243
C–O stretching, saturated aliphatic tertiary alcohols, SO_2 symmetric stretching, C=O stretching	1156
C–O–C symmetric and asymmetric stretching, esters of aromatic acids, saturated aliphatic ethers, C–O stretching, aliphatic secondary alcohols	1112
C–O stretching, saturated aliphatic primary alcohols	1069, 1041, 1029
C–H out of plane bending	989
N–O stretching, CH out of plane bending, vinyl esters	950.9
C–H out of plane bending	846
C–C stretching	738
Ring out of plane vibration o-substituted benzenes	506-450

700